Dentomaxillofacial Radiology (2020) 49, 20190445

birpublications.org/dmfr

TECHNICAL REPORT

Ultrasonography for diagnosis of peri-implant diseases and conditions: a detailed scanning protocol and case demonstration

[1]Hsun-Liang Chan and [2,3]Oliver D. Kripfgans

[1]Department of Periodontics and Oral Medicine, University of Michigan School of Dentistry, Ann Arbor, MI, USA; [2]Department of Biomedical Engineering, College of Engineering, Ann Arbor, MI, USA; [3]Department of Radiology, University of Michigan Medical School, Ann Arbor, MI, USA

Objectives: Ultrasonography has shown its promising diagnostic value in dental implant imaging research in the three treatment phases, namely, planning, intraoperative, and post-operative phase. With increasing awareness of peri-implant diseases and a lack of an efficient diagnostic method, the aim is to propose ultrasound imaging as a potential solution by providing a detailed scanning protocol and case demonstration.
Methods: Ultrasound device specification and the setup for optimizing peri-implant tissue imaging was described. Two useful imaging modes, viz. B-mode and color flow, were introduced. Important anatomical structures for accurate diagnosis of peri-implant diseases were illustrated. Finally, a detailed scanning sequence was proposed.
Results: Ultrasound images were acquired on live humans to exemplify the four peri-implant diseases and conditions, endorsed by the 2017 World Workshop organized by the American Academy of Periodontology and the European Federation of Periodontology. Ultrasound can provide not only cross-sectional anatomical images but also functional images (color flow images) that may be useful for evaluating the degree of peri-implant tissue inflammation.
Conclusions: High-frequency ultrasonography could be another cross-sectional imaging modality in adjunct to radiographs for diagnosing imminent peri-implant diseases and conditions that negatively influence quality of life of millions of patients with implants. This case study provides a framework for future related research work and clinical scanning guidelines.
Dentomaxillofacial Radiology (2020) **49**, 20190445. doi: 10.1259/dmfr.20190445

Cite this article as: Chan H-L, Kripfgans OD. Ultrasonography for diagnosis of peri-implant diseases and conditions: a detailed scanning protocol and case demonstration. *Dentomaxillofac Radiol* 2020; **49**: 20190445.

Keywords: ultrasonography; soft tissue; alveolar bone; peri-implantitis; dental Implants; cone-beam computed tomography

Introduction

The number of dental implants to replace missing teeth is rapidly increasing and has become the standard of care owing to a high survival rate. Successful implant treatment requires prudent clinical evaluations pre-surgically and post-functionally with high-quality images.[1,2] Unfortunately, peri-implant diseases and conditions occur frequently, with patients incurring significant financial burden and morbidity, especially when surgical repair is involved. According to a new classification,[3] there are two forms of peri-implant diseases, namely, "peri-implant mucositis" and "peri-implantitis." In addition, a condition named "hard and soft tissue deficiency around an implant" is identified. Peri-implant mucositis is analogous to gingivitis, featuring soft tissue inflammation but not progressive bone loss. On the other hand, peri-implantitis is similar to periodontitis, with continuous bone loss after initial bone remodeling. Depending on the disease definition threshold, the prevalence of peri-implant mucositis and peri-implantitis ranges from 19 to 65% and 1 to 47%, respectively.[4] The primary etiology of both diseases

Correspondence to: Dr Hsun-Liang Chan, E-mail: hlchan@umich.edu
Received 30 October 2019; revised 19 December 2019; accepted 28 January 2020

is a pathological biofilm on susceptible hosts. Peri-implant mucositis is believed to be reversible and can be treated with non-surgical mechanical means, with or without adjunctive chemical treatment. However, peri-implantitis is not reversible and requires surgical intervention to halt bone loss. The amount of bone loss follows a non-linear progressive pattern; therefore, early diagnosis and treatment is key to implant survival.[5,6]

The primary methods to diagnose peri-implant diseases and conditions are clinical examination and two-dimensional (2D) radiographs. Clinical probing usually underestimates disease severity because over contoured implant crowns usually interfere with probing access.[7] Bleeding on probing (BOP) is currently the only method to estimate the severity of clinical inflammation. However, it is neither objective nor sensitive enough to predict future bone loss.[8] Peri-apical films have high imaging resolution; however, their being 2D in nature limits their diagnostic value to mesial and distal sites. Facial and lingual/palatal bone loss is very common around implants but can't be revealed on 2D radiographs.[9,10] During the past decade, the use of cone beam CT (CBCT) is on the rise.[2] Being the only form of clinical cross-sectional imaging tool, CBCT provides clinically accurate hard tissue imaging; however, it needs to be used judiciously, due to its reliance on ionizing radiation. The American Academy of Oral and Maxillofacial Radiology states that routine use of CBCT for evaluating peri-implant health is not recommended due to radiation accumulation.[11] Other disadvantages include limited soft tissue contrast, higher cost, and suboptimal imaging quality from interfering artifacts created by metal objects.[12,13]

Non-ionizing, real-time and low-cost ultrasound has the potential to emerge as another useful cross-sectional imaging for peri-implant tissue evaluation.[14,15] It involves by definition acoustic waves with frequencies equal to or above 20 kHz, which are coupled and transmitted into the human body. Resulting images are based on acoustic waves that are scattered or reflected back to the transmitter as they encounter tissue interfaces. Depending on the time-of-fight t, *i.e.* the time the sound travels from the ultrasound probe into the body and reflects back to the same probe, the physical distance d is then computed as $d = c \cdot t$, where c is the sound speed in tissue. Ultrasound has been widely applied in medicine but has not gained acceptance in clinical dentistry. All related works have been restricted to pre-clinical and clinical research.[16–19] The major difficulty is a lack of high spatial resolution and small form factor ultrasound probes that can be used in the oral cavity.[20] Our recent cadaverous human study suggested feasibility of imaging peri-implant tissues by using a probe prototype.[14] In response to the imminent risks of peri-implant diseases, a new classification was developed and endorsed by the American Academy of Periodontology and European Federation of Periodontology in 2018.[3] In light of the limitations of current diagnostic methods, ultrasound images of four patients were demonstrated, each representing a specific implant disease or condition, along with introduction of a detailed ultrasound scanning protocol in this manuscript.

Methods and materials

Ultrasound scanner and probe setup

A commercially available ultrasound imaging device (ZS3, Mindray, Mountain View, CA) coupled with a 25 MHz (64 μm axial image resolution) and toothbrush-sized (~30 × 18 x 12 mm) probe prototype has been used for investigational intraoral scanning by our research team for a couple of years.[14] The same system was used to generate all the ultrasound images in this manuscript. Other systems on the market may also be used for scanning peri-implant tissue. After turning on the machine and registering the subject, "small parts examination" and the "superficial scanning" preset was selected to adapt to the features of peri-implant tissue. These functions optimize the ultrasound scanner to set transmit and receive parameters for the highest resolution, *i.e.* highest frequency, and are accompanied by setting the depth of field to 15 mm, which is adequate for most of instances in our experience because the soft tissue thickness seldom exceeds that number. Displaying the 15 mm depth on the screen creates optimal magnification, so even submillimeter structures can be visualized clearly. Additionally, to obtain good image resolution of specular reflectors such as alveolar bone, implant fixture, abutment and crown edges, "spatial compounding" was selected.[21] Acoustic coupling was achieved by the application of ultrasound gel and a gel-based stand-off-pad (Aquasonic, Parker Inc., PA).

Scanning modes

Still images and cine loops

As ultrasound is a real-time imaging modality, two types of images can be recorded and stored, namely, still images and cine loops. Still images refer to single 2D image frames; while cine loops are videos, *i.e.* a temporal collection of consecutive still images. A still image gives a snapshot of the field of view. Cine loops are useful when, *e.g.* a probe is either manually or mechanically moved cross-a volumetric region of interest. Cine loops are especially useful when tracing or confirming an anatomical structure is needed. In this case, one can translate or rotate the probe along or between structures to set them in spatial context with each other. Both image types can be saved in the Digital Imaging and Communications in Medicine format by default or other typical image and movie formats.

B-mode scan

B-Mode generates 2D images with the lateral and axial extend. The image content is composed of grayscale

pixels, where the degree of pixel "brightness," hence the letter "B," represents the backscattered (received) ultrasound echo in this particular axial/lateral location. The brightness is determined by the amplitude of the returned echo signal. B-mode images allow for visualization and quantification of spatial relations, including soft–hard tissue boundaries, various tooth and implant structures, and characterization of soft tissues as a result of backscatter changes. The lateral image dimension is defined by the probe width, and the axial extend is defined by the selected image depth of field. Regarding the image orientation, most of the time the top of the image is where the source of the ultrasound wave is originated from, *i.e.* the direction pointing to the ultrasound probe. Other image orientations are possible though unusual, such as the pediatric cardiac imaging. In this type of imaging, the direction to the probe is at the bottom side of the image, *i.e*. the image extends upwards into the patient's body.

Color flow scan

Blood flow can also be visualized using ultrasound. It is overlaid onto the B-mode display, which provides an anatomical reference. Blood-flow direction and relative velocity are imaged by selecting the color flow mode. Shades of red and blue colors are assigned to image pixels depending on the flow direction and velocity in a particular voxel. For normal ultrasound scanner operation, the colors red and blue illustrate blood towards and away from the transducer, respectively. The displayed images are not the actual *in situ* velocities, but rather their projection onto the imaging beams. Therefore, the displayed velocity is the actual velocity multiplied by the cosine of the enclosed angle. Blood flowing directly towards the ultrasound probe is displayed correctly as the enclosed angle is zero and cosine (0°) is unity. In contrary, a blood flow that is parallel to the probe surface is nearly invisible to the ultrasound as the enclosed angle is 90° and cosine (90°) equals zero. In practice, such flow is visualized due to finite beam and aperture effects and results in random red and blue voxels directly below the probe aperture.

The purpose of using color flow in the context of diagnosing peri-implant diseases is to quantify visible blood vessel density as a surrogate for the degree of inflammation. Blood flow data are filtered using a so-called *wall filter* to eliminate tissue motion. The term "*Wall"* refers here to the vascular wall of an artery, which typically displaces periodically with the heartbeat and would produce a strong artifact. The employed ultrasound scanner has three wall-filter settings: low, medium, and high. General wall filters can range from approximately 1–30% of the set velocity range. The upper end might seem excessive but is useful in cardiac imaging where tissue motion is inherently dominant and would generate artifactual color voxels. We choose low to filter a minimum amount of velocities, and thus reject velocities that are less than approximately 1–5% of the set velocity range, which we chose in the preset, *i.e*. 2.3 cm/s. Specific numerical values for the wall filter are not provided by this scanner. Other scanners may provide numerical values as percent, velocity or frequency.

Color power scan

Color power scan displays the strength, *i.e*. the intensity, of the signal in a single-hue color, typically red, rather than the speed and direction information.[22,23] It is particularly useful for small vessels and those with low-velocity flow. The signal is quantifiable, and its increase indicates higher blood volume, which may suggest inflammation. All three scanning modes, *i.e*. B-mode alone, color and color power, can be saved as "Still" or "Cine" images.

Scanning protocol

The scanning starts with a B-mode cross-sectional scan at the mid-facial site of an implant because most important anatomical landmarks can be identified for use to orient the examiner. These landmarks are implant crown outline (C), abutment surface (A), part of an implant fixture that is coronal to the bone (I), and the bone surface (B). Figure 1-Mid demonstrates such a scan on a healthy implant. The very top portion of an implant fixture is the implant platform (IP); the coronal end of the bone is the crestal bone (CB). The operator can adjust ultrasound probe angle and position in relation to the anatomy, with the probe placed approximately in line with the long axis of the implant, in order to capture all landmarks. At times, several B-mode still images may be needed to record all the landmarks. Afterward, the probe is slightly relocated mesially until the implant fixture/abutment complex is about to leave the field of view (Figure 1-Mesial). Another image could be taken when the mesial papilla becomes evident, that is, when the soft tissue surface starts to curve toward the palatal/lingual side. This image is very helpful for measuring the interdental papilla height and during the color flow and color power scans. On the distal site, the same approach as for the mesial site scans is applied. Peri-implant tissues can also be assessed on the palatal/lingual side with the same scanning methods. After the still scans, a cine scan across the width of the peri-implant space from the mesial to distal sites can be taken.

Results

Four clinical cases were used to demonstrate the four diseases and conditions of peri-implant tissues, defined by the American Academy of Periodontology/European Federation of Periodontology 2017 World Workshop on the Classifications of Periodontal and Peri-implant Diseases and Conditions.[3] These cases were part of a clinical trial evaluating short-term esthetic outcome of implants immediately placed with or without immediate provisionalization. The study was approved by

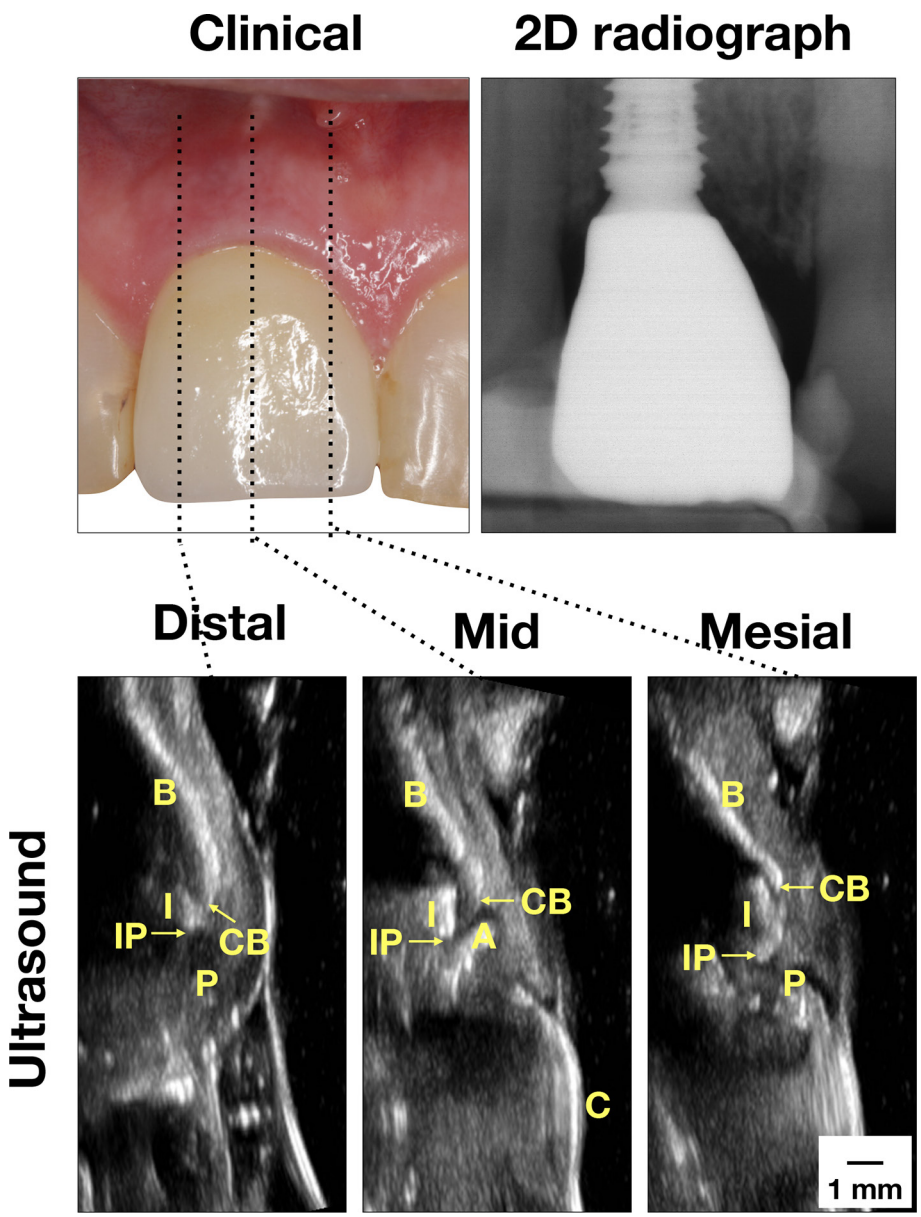

Figure 1 Case demonstration of a clinically healthy implant. Clinically, there are no signs of inflammation. Minimal bone loss was found on the peri-apical film. Ultrasound images on the mesial, mid-facial, and distal sites were presented. In the mid-facial image, the crown (C) surface is a bright line, connected to the abutment (A) and then the implant (I). The implant is readily identifiable because of the presence of the comet-tail artifact behind the implant. The bone surface (B) is yet another bright curved line. The junction between B and I is the CB. The junction between I and A is the IP. In the mesial and distal images, the bone and implant delineations are interpreted in the same way as in the mid-facial image. Additionally, the interdental papilla (P) is the structure between CB and the soft tissue surface. There is minimal implant fixture exposure, indicating normal bone level. CB,crestal bone; IP, implant platform.

the Investigational Review Board of The University of Michigan with the approval number HUM00139630 and registered in ClinicalTrials.gov with the Identifier NCT03558282. The case definition and diagnostic considerations are described below and summarized in Table 1.

(1) "Peri-implant health: (1) absence of peri-implant signs of soft tissue inflammation (redness, swelling, profuse bleeding on probing), and 2) the absence of further additional bone loss following initial healing."
(2) "Peri-implant mucositis: (1) presence of peri-implant signs of inflammation (redness, swelling, line or drop of bleeding within 30 s following probing), combined with 2) no additional bone loss following initial healing."
(3) "Peri-implantitis: (1) presence of peri-implant signs of inflammation, (2) radiographic evidence of bone

Table 1 Summary of case definition of peri-implant health, peri-implant mucositis, peri-implantitis and soft and hard tissue deficiencies. (+, presence; -, absence)

Clinical signs/ symptoms	*Case definition*	*Peri-implant health*	*Peri-implant mucositis*	*Peri-implantitis*	*Soft- and hard-tissue deficiencies*
Inflammation	Bleeding on gentle probing	-	+	+	+/-
	Erythema, swelling, and/or suppuration	-	+	+	-
Tissue loss	Increased probing depth	-	+	+	-
	Mucosal recession	-	-	+/-	+/-
	Bone loss beyond remodeling	-	-	+	+

loss following initial healing, and (3) increasing probing depth as compared to probing depth values collected after placement of the prosthetic reconstruction."

(4) "Hard and soft tissue deficiency" is not specifically defined by the 2017 Workshop. However, this condition represents diminished hard and soft tissue volume surrounding an implant, which may compromise implant longevity without overt inflammation.

Case one in Figure 1 represents "Peri-implant health," according to clinical and 2D radiographic findings (Table 2). The periodontal probing depth is 3 mm without BOP (lack of clinical inflammation). The radiographic marginal bone loss is 0.47 and 1.20 mm on the mesial and distal sites, respectively. This amount of bone loss is considered normal as a result of the host reaction in response to the surgical trauma and the foreign body (implant). In the mid-facial cross-sectional image, the crown (C) surface is a bright line, connected to the abutment (A) and then the implant (I). The implant is readily identifiable because of the presence of comet-tail artifact behind the implant. The bone (B) surface is yet another bright curved line. The junction between I and B is the CB. The junction between I and A is the IP. In the mesial and distal images, the bone and implant delineations are interpreted in the same way as in the mid-facial image. Additionally, the interdental papilla (P) is the structure between the CB and the soft tissue surface. Therefore, ultrasound images provide additional useful information, including the soft tissue height, soft tissue thickness, crestal bone thickness, and functional parameters, *e.g.* color flow and color power etc. The ultrasound soft tissue height, measured 2.9, 3.03, and 2.33 mm on the mesial, mid-facial, and distal sites, respectively, may correlate with the probing depth. The soft tissue thickness, measured 1.42 mm, and crestal bone thickness, measured 2.8 mm on the mid-facial site, are measures of tissue phenotype.

Case two in Figure 2 represents "Peri-implant mucositis." There is increased tissue inflammation and tissue swelling, as evidenced by visual examination and BOPs,

Table 2 Clinical, radiographic and ultrasound measurements of the four representative cases

Methods	*Parameters*	*Disease classification*			
		Peri-implant health	*Peri-implant mucositis*	*Peri-implantitis*	*Peri-implant soft- and hard-tissue deficiency*
Clinical	PD-m (mm)	3.0	3.0	3.0	3.0
	PD-mid (mm)	3.0	2.0	4.0	3.0
	PD-d (mm)	3.0	5.0	5.0	3.0
	BOP (positive sites/total six sites)	0	4	6	0
Radiographic	MBL-m (mm)	0.47	1.31	2.90	1.69
	MBL-d (mm)	1.20	0.96	1.71	1.68
Ultrasound-anatomical	STH-m (mm)[a]	2.90	3.55	3.86	4.13
	MBL-m (mm)	0.64	0.54	2.84	1.81
	STH-mid (mm)[a]	3.03	5.42	4.84	4.52
	MBL-mid (mm)[a]	1.37	2.30	1.07	2.32
	CBT-mid (mm)[a]	2.80	1.47	1.20	~0
	STT-mid (mm)[a]	1.42	1.74	2.11	0.74
	STH-d (mm)[a]	2.33	5.91	4.12	3.72
	MBL-d (mm)	1.74	0.59	1.31	1.27

BOP, bleeding on probing; CBT, crestal bone thickness; MBL, marginal bone loss;PD, probing depth; STH, soft tissue height; STT, soft tissue thickness; -d, distal site; -m, mesial site; -mid, mid-facial site of the studied implant.
[a]additional diagnostic values that ultrasound can provide beyond the current clinical and radiographic methods.

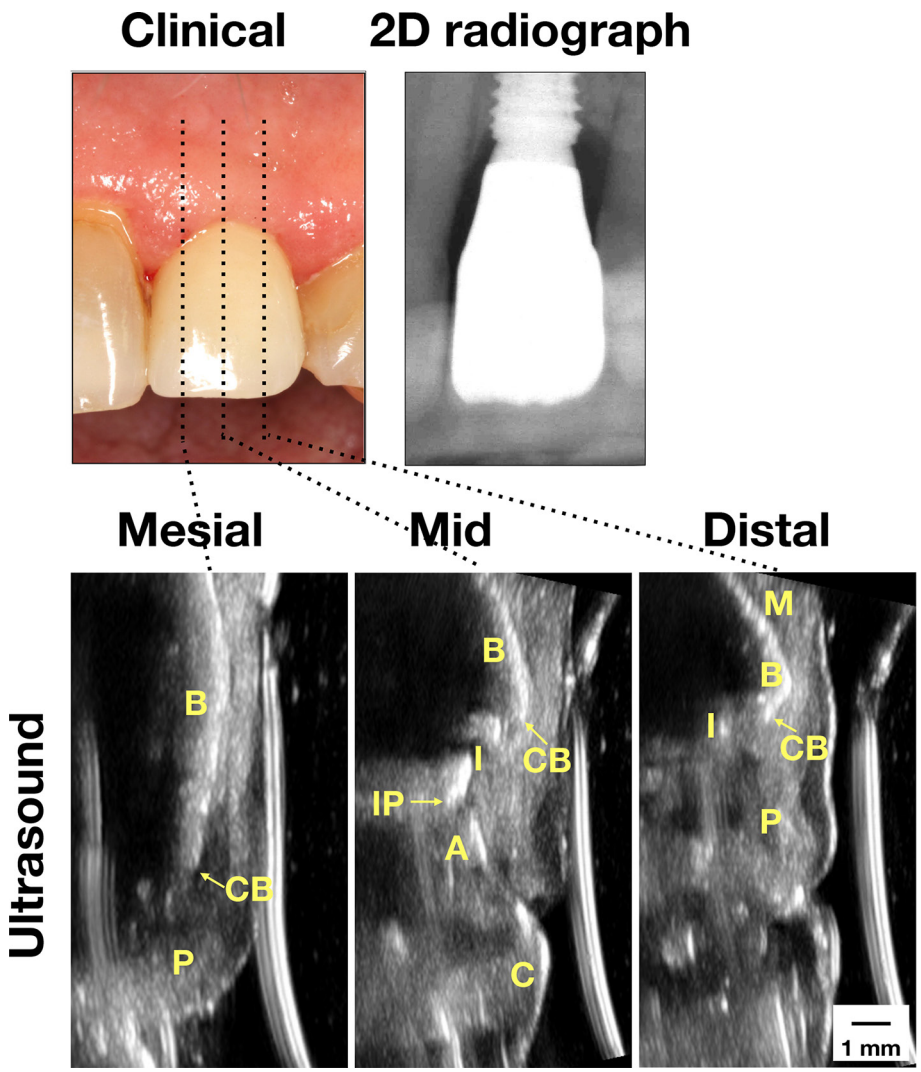

Figure 2 Case demonstration of an implant with peri-implant mucositis. Clinically, the mucosa swelled and bled upon probing. Normal bone level was found on the peri-apical film. Ultrasound images on the mesial, mid-facial, and distal sites showed normal bone level as well. 2D, two-dimensional; *A,* abutment; *B*, bone; C, crown; CB, crestal bone; *I,* implant; IP, implant platform; *M*, mucosa; *p,* papilla).

as well as increased probing depth, ranging from 2 to 5 mm (Table 2). Radiographic marginal bone loss, measured 1.31 and 0.96 mm on the mesial and distal sites, is within normal range as a result of the initial healing process. Ultrasound soft tissue height is measured 3.55, 5.42, and 5.91 mm. The remaining parameters are summarized in Table 2.

Case three in Figure 3 represents "Peri-implantitis." There is increased probing depth and tissue inflammation, ranging from 3 to 5 mm, with BOPs (Table 2). Radiographic marginal bone loss is more evident, with 2.9 and 1.71 mm on the mesial and distal sites, respectively. Ultrasound soft tissue height is 3.86, 4.84, and 4.12 mm on the mesial, mid-facial, and distal sites. Ultrasound marginal bone loss is 2.84, 1.07, and 1.31 mm on the mesial, mid-facial and distal sites. The crestal bone and soft tissue thickness on the mid-facial site is 1.2 and 2.11 mm, respectively.

Case four in Figure 4 represents "Peri-implant soft and hard tissue deficiency." The probing depth is within normal range (3 mm) without overt clinical inflammation. There is some radiographic marginal bone loss (1.69 and 1.68 mm on the mesial and distal sites, respectively) (Table 2). Ultrasound shows evidences of soft tissue deficiency, with 0.74 mm in soft tissue thickness, as well as hard tissue deficiency, with ~0 mm (below the axial resolution of 65 μm) in crestal bone thickness on the midfacial site. There is implant exposure, measured 2.32 mm on the mid-facial site. Additionally, there is a bony fenestration, evidenced by presence of implant threads at the more apical level.

Figure 5 illustrates color flow images at the mesial, mid-facial and distal sites of the four cases. As can be seen, the color intensity and extent are considerably less in the healthy case, compared to the other three cases.

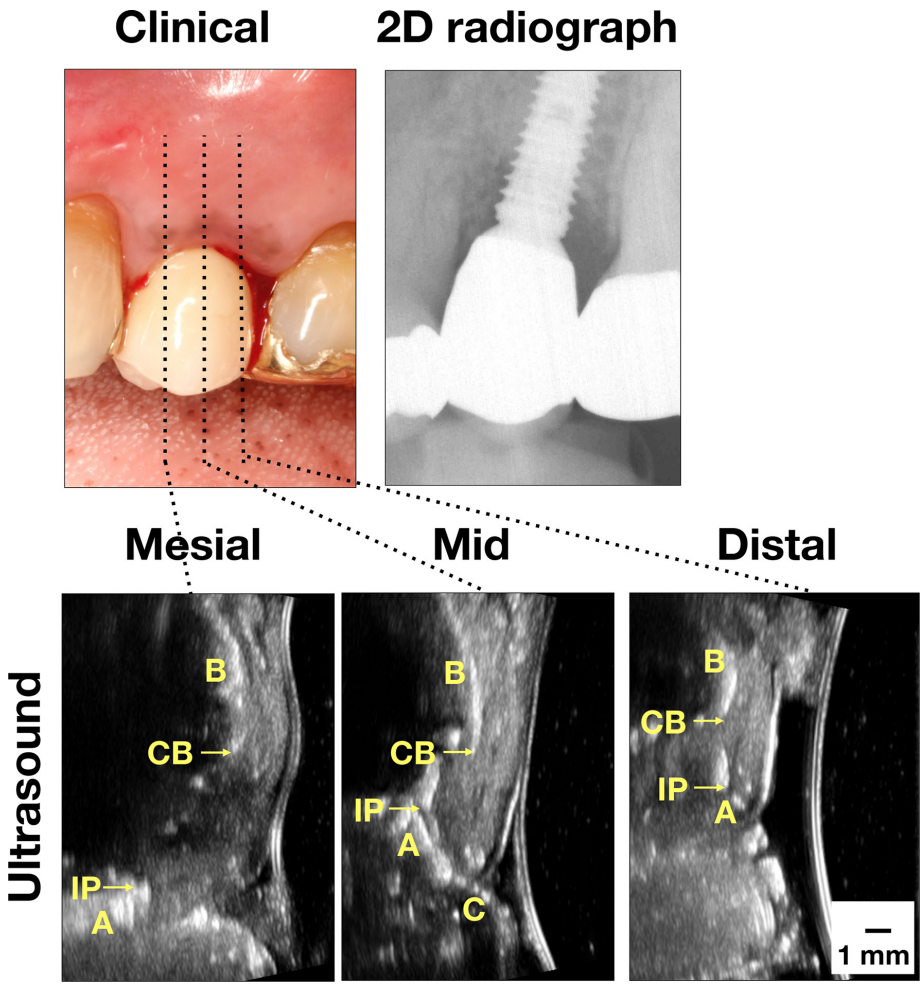

Figure 3 Case demonstration of an implant with peri-implantitis. Clinically, there were signs of inflammation, including bleeding on probing. Bone loss was obvious on the mesial site on the peri-apical film. Ultrasound images also showed bone loss. 2D, two-dimensional; *A,* abutment; *B*, bone; C, crown; CB, crestal bone; *I,* implant; IP, implant platform; *M,* mucosa; *p,* papilla).

The color flow may correlate with degree of peri-implant inflammation and may be related to BOP.

Discussion

This is the first attempt in the literature, to the authors' knowledge, to describe ultrasound technology and the scanning protocol in detail for the purpose of diagnosing peri-implant diseases and conditions. This promising technology displays images of peri-implant tissues of various health conditions in live humans with clinical and 2D radiographic data. Previous pre-clinical works by our research team have provided proof-of-principle that high-frequency ultrasound is accurate in measuring periodontal and peri-implant hard and soft tissue dimensions.[14,24,25] This manuscript further offers preliminary live-human data on using ultrasound to evaluate peri-implant tissues. Once validated by comparative studies with larger sample sizes, ultrasound could become a valuable diagnostic tool in patient care at chairside without ionizing radiation.

In a systematic review,[1] ultrasound was found potentially useful in various phases of implant therapy with different technology-development stages, ranging from benchtop studies to clinical trials. During the treatment-planning phase, knowledge of soft/hard tissue dimensions, tissue phenotype, relationship to vital structures, and bone density measurement is a pre-requisite for successful implant placement.[26–28] Ultrasound has been validated for measuring gingival thickness with a measurement deviation less than 10%.[29–31] During the surgery, ultrasound may be used to detect denser cortical bone that surrounds important structures; it could thus be used in lieu of radiographs to avoid surgical complications.[32–34] During the healing and maintenance phase, monitoring marginal bone level and implant stability is critical. This case study demonstrates the potential of ultrasound in identifying marginal bone level and implant structures that are necessary for linear

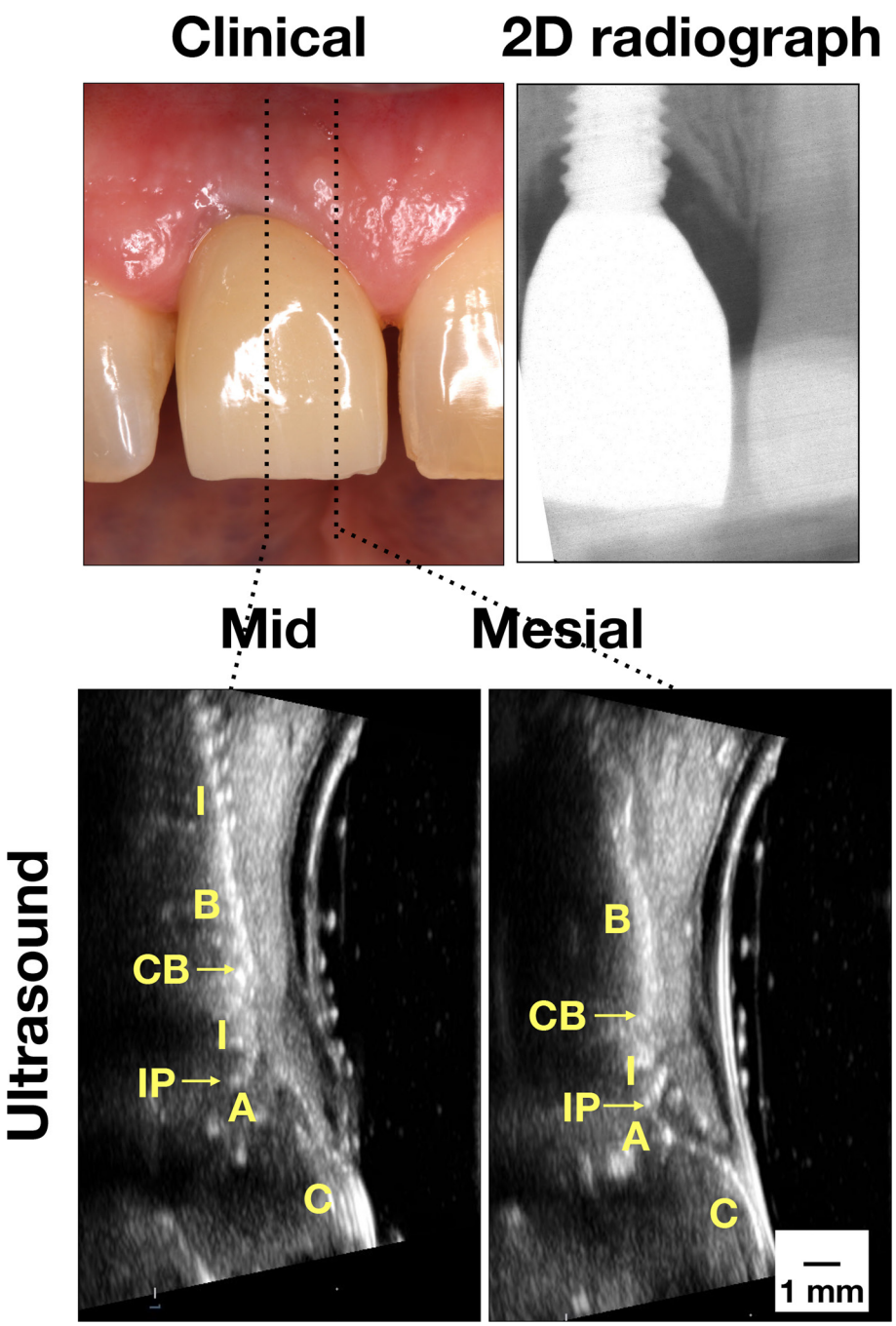

Figure 4 Case demonstration of an implant with hard and soft tissue deficiency. Clinically, there was slight inflammation. Some bone loss was found on the peri-apical film. Ultrasound images clearly showed thin mucosa and crestal bone, indicative of tissue deficiency. Implant exposure on the mid-facial view was evident. 2D, two-dimensional; *A,* abutment; *B,* bone; C, crown; CB, crestal bone; *I,* implant; IP, implant platform; *M,* mucosa; *p*, papilla.

bone-loss quantification. Basic ultrasound parameters, *e.g*. marginal bone loss and soft tissue height etc. obtained from B-mode images can already benefit peri-implant diagnosis.

Tissue phenotype is an important determinant of long-term implant function and esthetics. Thick peri-implant soft tissue can resist recession and camouflage metallic hue better than thin tissue.[27] Thin soft tissue phenotype and tissue recession can compromise implant function and esthetics, often requiring soft tissue graft surgery to correct this condition.[35] Adequate crestal bone thickness is desirable for maintaining bone homeostasis and soft tissue volume. Thin bone crest is less resistant to resorption due to biomechanical stress, *e.g*. occlusion and inflammation induced by bacterial biofilm. Therefore, additional ultrasound parameters

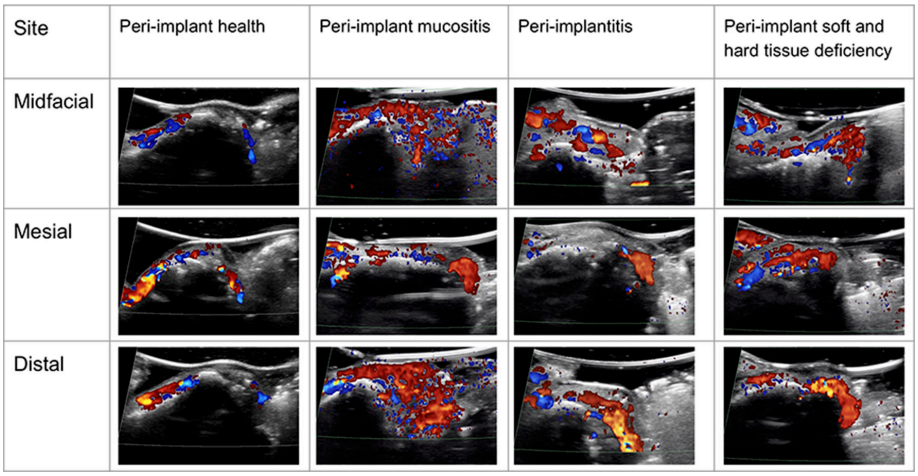

Figure 5 Color flow images of the four representative cases. The color intensity and extent within soft tissues is less in the peri-implant healthy case, compared to the other disease cases. Color follow may be used to evaluate the degree of inflammation.

that enable linear quantification of peri-implant soft and hard tissues in cross-sectional views can have a diagnostic value.

Functional ultrasound parameters, *e.g.* blood-flow imaging, may shed light on objective evaluation of peri-implant tissue inflammation. Bleeding on probing, the primary clinical method to estimate periodontal inflammation, is subjective and low in sensitivity.[8] In medicine, fractional blood volume has been studied to estimate inflammation.[36] Volumetric blood-flow imaging, as derived from three-dimensional color flow, is also an official biomarker of Quantitative Imaging Biomarkers Alliance.

The literature has shown that local blood flow increases at inflamed periodontal sites.[37] Color flow and color power modes can directly visualize flow as a function of space and yield fractional blood volume. These new imaging biomarkers could possibly detect subclinical inflammation before bone loss occurs. Timely interventions guided by early diagnosis could improve implant survival and patient-centered outcomes. Research is needed to validate these imaging biomarkers for quantifying peri-implant inflammation.

Limitations of ultrasound include the need for a medium for sound conduction, the inability to penetrate into bone, and a narrow field of view. High frequency ultrasound can image bone surfaces but not inside bone; therefore, ultrasound, as used here, is not intended to diagnose hard tissue pathology or intraosseous structures. Ultrasound is able to image a focused site in 2D but not the entire jawbone. Finally, since ultrasonic imaging is new to dentistry, a learning curve to adapt to this technology is required.

Acknowledgment

We would like to thank Mrs Alice Ou, RDH, MS, Clinical Research Coordinator, Department of Periodontics & Oral Medicine, University of Michigan School of Dentistry for participant recruitment and clincial data management.

Funding

The authors do not have any financial interests, either directly or indirectly, in the products or information listed in the paper. The study was supported by grants from the Delta Dental Foundation (PAF01878), the Osteology Foundation (PAF06301), Department of Periodontics and Oral Medicine Clinical Research Supplemental Research Grant, School of Dentistry Research Collaborative Award (U054647) and NIDCR R21 grant (1R21DE027765 - 01A1).

REFERENCES

1. Bhaskar V, Chan H-L, MacEachern M, Kripfgans OD. Updates on ultrasound research in implant dentistry: a systematic review of potential clinical indications. *Dentomaxillofac Radiol* 2018; **47**: 20180076. doi: https://doi.org/10.1259/dmfr.20180076
2. Chan H-L, Misch K, Wang H-L. Dental imaging in implant treatment planning. *Implant Dent* 2010; **19**: 288–98. doi: https://doi.org/10.1097/ID.0b013e3181e59ebd
3. Schwarz F, Derks J, Monje A, Wang H-L, Peri-implantitis WHL. Peri-Implantitis. *J Periodontol* 2018; **89**(Suppl 1): S267–90. doi: https://doi.org/10.1002/JPER.16-0350
4. Derks J, Tomasi C. Peri-Implant health and disease. a systematic review of current epidemiology. *J Clin Periodontol* 2015; **42**(Suppl 16): S158–71. doi: https://doi.org/10.1111/jcpe.12334
5. Chan H-L, Lin G-H, Suarez F, MacEachern M, Wang H-L. Surgical management of peri-implantitis: a systematic review

and meta-analysis of treatment outcomes. *J Periodontol* 2014; **85**: 1027–41. doi: https://doi.org/10.1902/jop.2013.130563
6. Khoshkam V, Chan HL, Lin GH, MacEachern MP, Monje A, Suarez F, et al. Reconstructive procedures for treating peri-implantitis: a systematic review. *J Dent Res* 2013; **92**(12 Suppl): 131S–8. doi: https://doi.org/10.1177/0022034513509279
7. Serino G, Turri A, Lang NP. Probing at implants with peri-implantitis and its relation to clinical peri-implant bone loss. *Clin Oral Implants Res* 2013; **24**: 91–5. doi: https://doi.org/10.1111/j.1600-0501.2012.02470.x
8. Hashim D, Cionca N, Combescure C, Mombelli A. The diagnosis of peri-implantitis: a systematic review on the predictive value of bleeding on probing. *Clin Oral Implants Res* 2018; **29**(Suppl 16): 276–93. doi: https://doi.org/10.1111/clr.13127
9. Correa LR, Spin-Neto R, Stavropoulos A, Schropp L, da Silveira HED, Wenzel A. Planning of dental implant size with digital panoramic radiographs, CBCT-generated panoramic images, and CBCT cross-sectional images. *Clin Oral Implants Res* 2014; **25**: 690–5. doi: https://doi.org/10.1111/clr.12126
10. Vandenberghe B, Jacobs R, Bosmans H. Modern dental imaging: a review of the current technology and clinical applications in dental practice. *Eur Radiol* 2010; **20**: 2637–55. doi: https://doi.org/10.1007/s00330-010-1836-1
11. Tyndall DA, Price JB, Tetradis S, Ganz SD, Hildebolt C, Scarfe WC, et al. Position statement of the American Academy of oral and maxillofacial radiology on selection criteria for the use of radiology in dental implantology with emphasis on cone beam computed tomography. *Oral Surg Oral Med Oral Pathol Oral Radiol* 2012; **113**: 817–26. doi: https://doi.org/10.1016/j.oooo.2012.03.005
12. Benavides E, Rios HF, Ganz SD, An C-H, Resnik R, Reardon GT, et al. Use of cone beam computed tomography in implant dentistry: the International Congress of oral Implantologists consensus report. *Implant Dent* 2012; **21**: 78–86. doi: https://doi.org/10.1097/ID.0b013e31824885b5
13. Mandelaris GA, Scheyer ET, Evans M, Kim D, McAllister B, Nevins ML, et al. American Academy of Periodontology best evidence consensus statement on selected oral applications for cone-beam computed tomography. *J Periodontol* 2017; **88**: 939–45. doi: https://doi.org/10.1902/jop.2017.170234
14. Chan H-L, Sinjab K, Li J, Chen Z, Wang H-L, Kripfgans OD. Ultrasonography for noninvasive and real-time evaluation of peri-implant tissue dimensions. *J Clin Periodontol* 2018; **45**: 986–95. doi: https://doi.org/10.1111/jcpe.12918
15. Chan H-L, Wang H-L, Fowlkes JB, Giannobile WV, Kripfgans OD. Non-ionizing real-time ultrasonography in implant and oral surgery: a feasibility study. *Clin Oral Implants Res* 2017; **28**: 341–7. doi: https://doi.org/10.1111/clr.12805
16. Marotti J, Heger S, Tinschert J, Tortamano P, Chuembou F, Radermacher K, et al. Recent advances of ultrasound imaging in dentistry – a review of the literature. *Oral Surg Oral Med Oral Pathol Oral Radiol* 2013; **115**: 819–32. doi: https://doi.org/10.1016/j.oooo.2013.03.012
17. Nguyen KC, Le LH, Kaipatur NR, Major PW. Imaging the cemento-enamel junction using a 20-mhz ultrasonic transducer. *Ultrasound Med Biol* 2016; **42**: 333–8. doi: https://doi.org/10.1016/j.ultrasmedbio.2015.09.012
18. Nguyen KC, Le LH, Kaipatur NR, Zheng R, Lou EH, Major PW. High-Resolution ultrasonic imaging of Dento-Periodontal tissues using a Multi-Element phased array system. *Ann Biomed Eng* 2016; **44**: 2874–86. doi: https://doi.org/10.1007/s10439-016-1634-2
19. Nguyen K-CT, Pachêco-Pereira C, Kaipatur NR, Cheung J, Major PW, Le LH. Comparison of ultrasound imaging and cone-beam computed tomography for examination of the alveolar bone level: a systematic review. *PLoS One* 2018; **13**: e0200596. doi: https://doi.org/10.1371/journal.pone.0200596
20. Ghorayeb SR, Bertoncini CA, Hinders MK. Ultrasonography in dentistry. *IEEE Trans Ultrason Ferroelectr Freq Control* 2008; **55**: 1256–66. doi: https://doi.org/10.1109/TUFFC.2008.788
21. Entrekin RR, Porter BA, Sillesen HH, Wong AD, Cooperberg PL, Fix CH. Real-time spatial compound imaging: application to breast, vascular, and musculoskeletal ultrasound. *Seminars in Ultrasound, CT and MRI* 2001; **22**: 50–64. doi: https://doi.org/10.1016/S0887-2171(01)90018-6
22. Rubin JM, Adler RS, Fowlkes JB, Spratt S, Pallister JE, Chen JF, et al. Fractional moving blood volume: estimation with power Doppler US. *Radiology* 1995; **197**: 183–90. doi: https://doi.org/10.1148/radiology.197.1.7568820
23. Rubin JM, Bude RO, Carson PL, Bree RL, Adler RS. Power Doppler US: a potentially useful alternative to mean frequency-based color Doppler US. *Radiology* 1994; **190**: 853–6. doi: https://doi.org/10.1148/radiology.190.3.8115639
24. Chan H-L, Sinjab K, Chung M-P, Chiang Y-C, Wang H-L, Giannobile WV, et al. Non-invasive evaluation of facial crestal bone with ultrasonography. *PLoS One* 2017; **12**: e0171237. doi: https://doi.org/10.1371/journal.pone.0171237
25. Tattan M, Sinjab K, Lee E, Arnett M, TJ O, Wang HL, et al. Ultrasonography for Chairside evaluation of periodontal structures: a pilot study. *Journal of periodontology* 2019;.
26. De Rouck T, Eghbali R, Collys K, De Bruyn H, Cosyn J. The gingival biotype revisited: transparency of the periodontal probe through the gingival margin as a method to discriminate thin from thick gingiva. *J Clin Periodontol* 2009; **36**: 428–33. doi: https://doi.org/10.1111/j.1600-051X.2009.01398.x
27. JH F, Lee A, Wang HL. Influence of tissue biotype on implant esthetics. *The International journal of oral & maxillofacial implants* 2011; **26**: 499–508.
28. Kan JYK, Morimoto T, Rungcharassaeng K, Roe P, Smith DH. Gingival biotype assessment in the esthetic zone: visual versus direct measurement. *Int J Periodontics Restorative Dent* 2010; **30**: 237–43.
29. Culjat MO, Choi M, Singh RS, Grundfest WS, Brown ER, White SN. Ultrasound detection of submerged dental implants through soft tissue in a porcine model. *J Prosthet Dent* 2008; **99**: 218–24. doi: https://doi.org/10.1016/S0022-3913(08)60046-3
30. Culjat MO, Choi M, Singh RS, White SN. Ultrasound imaging of dental implants. Conference proceedings : Annual International Conference of the IEEE Engineering in Medicine and Biology Society. *IEEE Engineering in Medicine and Biology Society Annual Conference* 2012; **2012**: 456–9.
31. Traxler M, Solar P, Ulm C, Gritzmann N. Ultrasonographic measurement of the soft-tissue of the upper jaw. *Acta Radiol* 1991; **32**: 3–5. doi: https://doi.org/10.1177/028418519103200102
32. Machtei EE, Zigdon H, Levin L, Peled M. Novel ultrasonic device to measure the distance from the bottom of the osteotome to various anatomic landmarks. *J Periodontol* 2010; **81**: 1051–5. doi: https://doi.org/10.1902/jop.2010.090621
33. Rosenberg N, Craft A, Halevy-Politch J. Intraosseous monitoring and guiding by ultrasound: a feasibility study. *Ultrasonics* 2014; **54**: 710–9. doi: https://doi.org/10.1016/j.ultras.2013.09.008
34. Zigdon-Giladi H, Saminsky M, Elimelech R, Machtei EE. Intra-operative measurement of the distance from the bottom of osteotomy to the mandibular canal using a novel ultrasonic device. *Clin Implant Dent Relat Res* 2016; **18**: 1034–41. doi: https://doi.org/10.1111/cid.12362
35. Zucchelli G, Tavelli L, Stefanini M, Barootchi S, Mazzotti C, Gori G, et al. Classification of facial peri-implant soft tissue dehiscence/deficiencies at single implant sites in the esthetic zone. *J Periodontol* 2019; **90**: 1116–24. doi: https://doi.org/10.1002/JPER.18-0616
36. Terslev L, Torp-Pedersen S, Qvistgaard E, Danneskiold-Samsoe B, Bliddal H. Estimation of inflammation by Doppler ultrasound: quantitative changes after intra-articular treatment in rheumatoid arthritis. *Ann Rheum Dis* 2003; **62**: 1049–53. doi: https://doi.org/10.1136/ard.62.11.1049
37. Cekici A, Kantarci A, Hasturk H, Van Dyke TE. Inflammatory and immune pathways in the pathogenesis of periodontal disease. *Periodontol 2000* 2014; **64**: 57–80. doi: https://doi.org/10.1111/prd.12002